EUROPEAN FUSION DEVELOPMENT AGREEMENT

EFDA–JET–CP(04)02/17

R.A. Pitts, P. Andrew, X. Bonnin, A.V. Chankin, Y. Corre, G. Corrigan,
D. Coster, I. Duran, T. Eich, S.K. Erents, W. Fundamenski, A. Huber,
S. Jachmich, G. Kirnev, M. Lehnen, P.J. Lomas, A. Loarte, G.F. Matthews,
J. Rapp, C. Silva, M.F. Stamp, J.D. Strachan, E. Tsitrone
and JET EFDA contributors

Edge and Divertor Physics with Reversed Toroidal Field in JET

Edge and Divertor Physics with Reversed Toroidal Field in JET

R.A. Pitts[1], P. Andrew[2], X. Bonnin[3], A.V. Chankin[4], Y. Corre[3], G. Corrigan[2], D. Coster[4], I. Duran[5], T. Eich[4], S.K. Erents[2], W. Fundamenski[2], A. Huber[6], S. Jachmich[7], G. Kirnev[8], M. Lehnen[6], P.J. Lomas[2], A. Loarte[9], G.F. Matthews[2], J. Rapp[6], C. Silva[10], M.F. Stamp[2], J.D. Strachan[11], E. Tsitrone[3]
and JET EFDA contributors[*]

[1]Centre de Recherches en Physique des Plasmas, Association Euratom-Confédération Suisse, Ecole Polytechnique Fédérale de Lausanne, CH-1015 Lausanne, Switzerland
[2]Euratom/UKAEA Fusion Association, Culham Science Centre, Abingdon, OX14 3DB, UK
[3]Association EURATOM-CEA, CEA Cadarache, 13018 St. Paul lez Durance, France.
[4]Max-Planck-Institut für Plasmaphysik, EURATOM-Association, Boltzmann Str. 2., D-85748, Garching, Germany
[5]Institute of Plasma Physics, Association EURATOM-IPP.CR, Prague, Czech Republic
[6]FZJ Julich GmbH/Euratom Institut für Plasmaphysik, TEC, Julich D-52425 Germany
[7]LPP, ERM/KMS, Association Euratom-Belgian State, B-1000, Brussels, Belgium
[8]Moscow Nuclear Fusion Institute, RRC "Kurchatov Institute", 123182 Moscow, Russia
[9]EFDA-CSU, Max-Planck-Institut für Plasmaphysik, D-85748, Garching Germany
[10]Associção Euratom-IST, Av. Rovisco Pais, 1049-001 Lisbon, Portugal
[11]Plasma Physics Laboratory, Princeton University, Princeton, NJ 08543, USA
** See annex of J. Pamela et al, "Overview of Recent JET Results and Future Perspectives", Fusion Energy 2002 (Proc. 19th IAEAFusion Energy Conference, Lyon (2002).*

Preprint of Paper to be submitted for publication in Proceedings of the
16th PSI Conference,
(Portland Maine, USA 24-28 May 2004)

ABSTRACT

Asymmetries are a ubiquitous feature of the Scrape-Off Layer (SOL) and divertor plasmas in any tokamak and are thought to be driven primarily by a variety of drift flows, the directions of which reverse with reversal of the main toroidal field. The understanding of precisely how these field dependent effects combine to yield any given experimental observation is still very much incomplete. A recent campaign of reversed field operation at JET designed to match a variety of discharges to their more frequently executed forward field counterparts has been executed in attempt to contribute to this understanding in the key areas of SOL flow and divertor asymmetries. This paper summarises the most important findings from these experiments and includes some new EDGE2D simulation results describing the SOL flow.

1. INTRODUCTION

The 1999 ITER physics basis [1] addresses Scrape-Off Layer (SOL) and divertor drift flows only superficially, noting that they "are not yet routinely included in two-dimensional modelling". This is still true concerning ITER simulations and, five years on, much remains to be understood not just of the drift flows themselves but also, and perhaps more importantly, of their consequences for critical issues impacting ITER design and operation such as material migration [2] and divertor asymmetries. There has, however, been notable recent progress in the experimental characterisation of tokamak SOL and divertor flows, particularly the increased poloidal coverage in C-Mod [3] and JT-60U [4]. In the latter case, some advance has also been achieved in matching the results of numerical modelling using the UEDGE fluid code including classical drifts to experimental data.

All classical particle cross-field drifts reverse direction upon reversal of the toroidal magnetic field, B_φ, so that comparing experimental results obtained from discharges as closely matched as possible in everything but the direction of B_φ is the most obvious method by which at least some of the drift effects may be disentangled. Such experiments have been reported from a number of facilities [5-7], including JET [8], from which the principal results of the most recent field reversal campaign provide the content of this paper. A number of companion papers within these proceedings discuss in more detail some aspects of the material covered here. They are appropriately referenced throughout the text.

2. EXPERIMENTAL DETAILS

Like many tokamaks, standard plasma operation at JET is performed with B_φ *negative*, which, in a right-handed cylindrical coordinate system (r, φ, z) with z pointing vertically upwards, means that the ion B×∇B drift direction points downwards. Henceforth, this "normal" toroidal field direction will be referred to as"*forward* field to distinguish it from the "abnormal" or positive B_φ, denoted here as *reversed* field.

In JET, the divertor target tile design requires that field lines impact always from the same direction and thus that the plasma current, I_p, be reversed simultaneously with B_φ. With the exception

of a few H-mode cases in reversed field, additional heating in the discharges has been performed exclusively with neutral beam injection. In reversed B_φ, beam injection is therefore in the counter Ip direction. Independent of field direction, all data reported here have been obtained from plasma operation in the MarkIISRP Gas Box divertor configuration with vacuum vessel wall temperature 200°C and deuterium gas fuelling only.

In recent years at JET a magnetic equilibrium which allows for optimum coverage of the edge and SOL regions with the available diagnostics has been developed and much exploited [9]. This Diagnostic Optimised Configuration (DOC-L) with strike points on the lowest of the two sets of vertical target tiles in the inner and outer divertors (see inset in Fig.1) has been used for many of the reversed B_φ comparison discharges. By always selecting similar magnitudes of I_p and B_φ, the edge safety factor remains largely unchanged throughout the database - the range $3 < q_{95} < 4$ encompasses most discharges, the majority of which have been executed for three principal combinations of (I_p[MA], B_φ[T]): ±(1.2, 1.2), ±(2.0, 2.4) and ±(3.0, 3.0).

Scrape-off layer flows on JET (Section 3) are measured using fast reciprocating probe systems equipped with Mach probe heads, whilst divertor parameters (Section 4) are monitored by tile embedded thermocouples and Langmuir probes, IR thermography and divertor spectroscopy including total radiation bolometry and volume averaged fuel and impurity line emission intensities. Numerical modelling in support of this data is being performed by the EDGE2D/Nimbus and SOLPS5 code packages.

3. SOL FLOW

Parallel SOL flow measurements have been previously reported from JET, along with some early code simulations including drift effects [10]. The more recent experiments discussed here consolidate and significantly improve on the older results. Modelling has similarly advanced in the sense that convergence with drifts in the earlier simulations yielded solutions for rather unrealistic conditions, inappropriate to experiment.

3.1 EXPERIMENT

In common with the experiments of [10], parallel flow is measured from the top, Low Field Side (LFS) of the JET poloidal cross-section. Two fast reciprocating drives are installed at this position, toroidally separated by 180°. Each carries a different probe head, the first a bidirectional retarding field analyser (RFA) [11] and the second a Turbulent Transport Probe (TTP) [12]. Both have pairs of sensing elements facing the inner and outer divertors along field lines and can therefore be used as Langmuir probes from which the plasma flow parallel to the total magnetic field can be estimated from the ratio of the ion particle flux densities to each side of the device. Here, as elsewhere [3,4, 10], this flow is computed according to the expression due to Hutchinson [13]: $M_{||} = 0.4\ln(j_{sato}/j_{sati})$, where $M_{||} = v_{||}/cs$ with $v_{||}$ the parallel ion fluid flow speed, c_s the sound speed ($c_s = \sqrt{e(T_e + T_i)/m_i}$ for T_i, T_e in eV) and j_{sato}, j_{sati} the ion saturation current densities to probe elements facing the outer or inner

divertors respectively. In the definition used here, positive $M_{||}$ corresponds to a flow past the probe in the direction from outer to inner divertor.

When appropriate radial shifts are applied, both probes yield similar radial $M_{||}$ profiles in identical plasma conditions. An example is presented in Fig.1 from the RFA probe for closely matched forward and reversed B_φ ohmic discharges [14]. The essential features of Fig.1 are retrieved in additionally heated L-mode discharges, though the operational difficulties of using these probes in high power conditions prevent reliable measurements in H-mode.

There are several important observations to be drawn from Fig.1: the forward B_φ flow is always positive, reaching high values, $M_{||} \sim 0.5$, in the main SOL and rising from a somewhat lower value, $M_{||} \sim 0.2$ near the separatrix. Upon field reversal, in this example, the flow is mostly stagnant ($M_{||} \sim 0$) in the SOL but rises to the forward field value near the separatrix and thus remains directed towards the inner divertor. Field reversal therefore flips the forward B_φ profile about an offset value of $M_{||} \sim 0.2$ which is approximately constant across the SOL.

Further evidence that the RFA measured strong flow does in fact exist is provided by the ion temperatures, T_{ii}, T_{io}, measured by the RFA itself in the directions facing inner and outer divertors. Example radial profiles are presented in Fig.2 for a range of discharges with varying density in both field directions. In forward field, $T_{io} > T_{ii}$ generally applies, whilst $T_{io} \sim T_{ii}$ in reversed field. This asymmetry is precisely what has recently been predicted to occur in the case of a bi-directional RFA immersed in a flowing plasma [15]. In effect, it is the probe itself that perturbs the local plasma by depleting ions preferentially on the downstream side of the flow, generating strong electric fields and modifying the ion velocity distribution. For forward B_φ, the T_{io}/T_{ii} ratios derived from Fig.2 are in reasonable quantitative agreement with theoretical expectation if the flow is of the magnitude shown in Fig.1 [16]. In reversed field, $T_{io}/T_{ii} \sim 1$, as expected for approximately stagnant flow.

3.2 MODELLING

Parallel flow is generated in a torus due to poloidal asymmetries of the toroidal field, radial and poloidal electric fields and pressure gradients. Combining all contributing effects can only really be accomplished by code simulation. The preliminary attempts reported in [10] to model JET the SOL with drift terms included have been considerably extended in seeking agreement with the new flow data [14]. As before, simulations are being pursued with the EDGE2D/Nimbus code package [17] with all important particle drifts ($E\times B$, $B\times\nabla B$, curvature) activated. Drift terms are applied to both fuel and impurity (carbon) species and are active across the simulation grid from the inner core boundary across the separatrix and into the SOL. Radial profiles of $D_\perp$ and $\chi_\perp$ are specified with $\chi_\perp(r) = 2D_\perp(r)$ such that the best possible match is obtained between upstream and downstream (divertor target) profiles of T_e and n_e. Main chamber gas puffing with separatrix density control is used in the code, as in experiment, and supersonic boundary conditions are allowed at the target plates.

Results for the predicted SOL flow at the probe location but with the radial coordinate mapped, by convention, to the outer midplane (as also in Figs.1-3) are compiled in Fig.3(a). They are appropriate to the discharge conditions under which the data of Fig.1 were obtained. Although the experimental trend with both radius and density is approximately reproduced when drifts are included, the predicted values of $M_{||}$ are too low by a factor of between 5-10. The situation is considerably worse when drift terms are switched off. Despite the improved numerical simulations, the essential conclusion is thus unchanged from that reached previously [10] - the forward B_φ flow magnitude is not matched by the code.

Concerning the apparent offset, one obvious candidate is a parallel compensatory flow that might arise from enhanced radial transport due to ballooning in the outboard region of unfavourable curvature. Such a flow would be naturally field independent and would not be observed by midplane located probes such as those on C-Mod [3] or JT-60U [4]. If sufficiently large it should, however, be registered by a measurement further away poloidally. Unfortunately, the $M_{||} \sim 0.2$ offset seen in the JET data would appear to be inconsistent with EDGE2D simulations which, whilst matching midplane measurements of D_α emisison, predict a total core particle efflux which is nearly an order of magnitude too small to account for the integrated parallel ion flux measured by the probe [14].

Several avenues are being explored that might explain all or part of the discrepancy between code and experiment. The first is to thoroughly benchmark EDGE2D and SOLPS5.0 - the two major codes in use at JET [18]. At the time of writing, although SOLPS5.0 runs including drifts have begun and are showing encouraging initial signs of agreement with EDGE2D, the results are insufficiently mature for meaningful conclusions to be drawn.

A second postulates a convective transport pinch in the SOL and pedestal region, together with a ballooning-like poloidal variation of particle outflux ($D_\perp \propto 1/B_\varphi$) [19]. The pinch term is assumed to originate from a radial $E_\theta \times B_\varphi$ velocity and is directed inwards on the high field side (HFS) and outwards on the LFS for forward B_φ. As shown in Fig.3(b), introducing such transport into EDGE2D (without drifts) does indeed yield high parallel flows directed from outer to inner targets at the probe location.

In a third approach, the perturbing effect of the probe itself is invoked as a mechanism by which the background flow might be amplified. This possibility is inspired by the intense impurity “plumes” which are always observed on visible CCD camera images of the plasma cross-section when the probes reciprocate. Such plumes, deliberately introduced, have in fact been used elsewhere to diagnose the presence of SOL flow [6]. The local radiation in the case of the JET probes originates principally from impurities released from the carbon coated, boron nitride probe heads by physical and possibly chemical sputtering. By introducing an atomic carbon source in grid cells adjacent to the nominal probe location, the situation may be modelled very approximately using EDGE2D [14]. The code indicates the establishment of a steep local parallel temperature gradient which can drive rather strong flow in forward B_φ (Fig.3(b)). If true, flow generation in this way has worrying implications for measurements reported elsewhere, the majority of which make recourse to the

same probe technique and which, more often than not, yield flows greater than can be accounted for by established theory.

Finally, a pragmatic attitude can be adopted in which the probe measurements are taken at face value with the admission that the mechanism(s) driving the flow are not yet understood. A poloidally distributed, external momentum source is specified in the EDGE2D simulations such that the experimental flows are reproduced by the code. Such an approach has been successfully applied in attempting to model the results of CH_4 screening experiments in matched forward and reversed field discharges [20].

4. DIVERTOR ASYMMETRIES

A number of divertor asymmetry aspects have been addressed by this reversed field campaign. They may be very broadly divided into power and particle asymmetries and are discussed here mostly within the context of the database of DOC-L discharges mentioned in Section 2.

4.1 POWER

Due to progressive loss of divertor Langmuir probes over previous campaigns, only in a few reversed B_φ dedicated pulses with vertical strike point sweeping have target profiles been obtained for comparison with previous matched forward B_φ cases [21]. In general, for both L and H-mode, field reversal leads to more symmetric divertor plasmas with $T_{e,\,inner} \sim T_{e,\,outer}$, in constrast to the case of forward B_φ, in which the inner target is almost always partially or fully detached even at comparatively low densities. Similar trends are seen when studying carefully matched L-mode density limit discharges [22], for which the reversed B_φ density limit is found to be ~20% lower than in forward field.

An extremely robust diagnostic of divertor energy asymmetry is provided by a set of target tile embedded thermocouples (see inset in Fig.4(b)), data from which are available for every JET discharge and which are used to estimate the integral energy deposition on each tile for each pulse. Only a single data point is thus available for each shot. This data is compiled in Fig.4(a) in the form of the outer to inner divertor energy asymmetry, E_A, as a function of integrated total energy into the SOL, $E_{SOL} = E_{IN} - E_{RAD}$, with E_{IN}, E_{RAD} respectively the total energy input and radiated throughout the diverted phase of the discharge. The database contains a total of 110 DOC-L discharges with $|B_\varphi|$ in the range 1.2-3.0T. Separation into confinement groups is performed crudely by assigning an H-mode label to discharges containing a prolonged Type I ELMing phase.

Whilst its magnitude is not delineated in Fig.4(a), there is a very obvious dependence on the *sign* of B_φ. Beginning from a common "offset" value at $E_A \sim 2.2$ for low ESOL, the asymmetry increases roughly linearly with E_{SOL} for forward B_φ and decreases with reversed B_φ. The dependence on E_{SOL} is steeper for L-mode than H-mode for both field directions and is strongest for L-mode reversed field plasmas. An average of EA across both field directions for all ESOL yields an approximately constant value close to the initial offset. This is

unsurprising given the geometrical factor afforded by the toroidal geometry (~1.6 for these discharges), by which more power reaches the SOL on the LFS than the HFS, the tendency for enhanced cross-field transport (ballooning) in the LFS region of bad curvature and a possible further contribution deriving from the compression of flux surfaces on the LFS (Shrafanov shift) which would favour enhanced cross-field heat flux there if the latter were proportional to radial gradients [23].

Bolometric reconstructions of divertor radiation for a few matched discharge pairs [21, 22] indicate that the in/out distribution is relatively insensitive to field direction and certainly cannot be responsible for a large fraction of the observed E_A. This is entirely consistent with the reported findings from an earlier reversed field campaign on JET with the Mark I divertor geometry [8]. Since all H-mode points in Fig.4(b) are associated with Type I ELMs, the temptation is to ascribe the reduction of E_A for both field directions to the ELMs themselves.

Whilst there must certainly be some truth to this supposition, an equal contribution might also be due to changes in EA during ELM-free phases. In principle, the advanced IR thermography systems on JET are capable of deriving the ELM and ELM-free target power fluxes, but analysis is complicated by the presence of surface layer accumulation due to impurity deposition (see below and [24]).

Although limited to a single data point per discharge, the thermocouple data can nevertheless be used to demonstrate clearly that heat flux drifts must be largely responsible for the observed variation of E_A with E_{SOL}. The conclusions drawn here on the basis of a larger data sample are entirely supported by, and in fact rely upon, the results of a more detailed study restricted to the vertical strike point swept discharges referred to earlier [21]. There, it is demonstrated that the scaling $\lambda_q \propto P_{SOL}^{-0.4} B_\varphi^{-1} n_u^{0.25}$ for the SOL energy scrape-off width (n_u is the upstream separatrix density) found in an extensive study in forward field [25], is also preserved in reversed field. The radial energy transport is then essentially independent of field direction. This study has also clearly demonstrated by using ASCOT code modelling that ion orbit loss cannot be a major contributor to the observed energy asymmetries [21].

It can be shown [23], that for $T_i = T_e$, the ratio of the diamagnetic and E×B drift fluxes in the poloidal and radial directions (strictly the diamagnetic direction but the difference will be ignored here) to the expected (in the absence of drifts) parallel and radial fluxes scales as $\rho_{i\theta}/\lambda$, with λ the characteristic SOL length for density or temperature (for particle or heat fluxes) and $\rho_{i\theta}$ is the ion poloidal gyro-radius. For forward B_φ, these poloidal drift fluxes are in the direction from inner to outer target, reversing direction with B_φ reversal and would thus be in the right direction to reinforce the baseline asymmetry in forward field and reduce it for reversed B_φ. Since the database discharges are selected for a restricted range of safety factor (Section 2), B_φ may be used to replace B_θ in the expression for Larmor radius: $\rho_{i\theta} = cs/w_{i\theta} = c_s m_i/eB_\theta \propto \sqrt{T_i}/B_\varphi$, so that the contribution of drifts to heat flux transport in the SOL might be expected to scale approximately as, $T_u^{0.5} B_\varphi^{-1} \lambda_q^{-1}$, with T_u the upstream separatrix temperature. Inserting the scaling for λ_q mentioned above leads to a drift

effect $\propto T_u^{0.5} P_{SOL}^{0.4} n_u^{-0.25}$ with no B_φ dependence! Given that T_u is generally unavailable, it can be expressed in terms of a power per particle: $\propto P_{SOL}/n_u$, yielding a final drift effect $\propto P_{SOL}^{0.9} n_u^{-0.75} \sim P_{SOL}/n_{e,\,vol}$ Passuming a linear relationship between n_u and the volume averaged density [26]. In Fig.4(b), E_A is plotted against a modified version of this quantity: $\text{sign}(B_\varphi)\langle P_{SOL}\rangle/\langle n_{e,\,vol}\rangle$ where $\langle n_{e,\,vol}\rangle$ is the average of $n_{e,\,vol}$ over the diverted phase of the discharge and $\langle P_{SOL}\rangle$ is the "energy weighted power", $\int P_{SOL}\,dE/\int dE$, which more properly accounts for the fact that for the thermocouples, longer phases at lower heating power are equivalent to shorter phases at higher power. Negative values on the abscissa of Fig.4(b) correspond to forward B_φ and, unlike in Fig.4(a), the points are now differentiated not only according to confinement regime but also to $|B_\varphi|$.

The fact that the data cluster approximately about a straight line extending either side of the low P_{SOL} offset value mentioned above is strong evidence that field dependent drift effects are responsible for the variations of E_A in this dataset. Since both diamagnetic and E×B drifts scale in the same way with input power, it is not possible from these measurements to infer the relative contribution of each. Nor has this simple analysis accounted for the strong drift fluxes known to occur in the divertor itself [4,27], convecting particles and heat through the private flux region (PFR).

4.2 PARTICLES

The general trend toward symmetrisation of divertor recycling fluxes is illustrated in Fig.5(a), again using the DOC-L database but on this occasion making use of the spectroscopic data which, unlike the thermocouple energies, is available at all times through the discharge. A number of time windows of duration 0.5s are selected in each discharge and the data averaged within this period. The chosen interval is long enough for several ELMs to be included in the average if the window falls within an H-mode phase. In Fig.5(a), the ratio of calibrated D_α fluxes is obtained from lines of sight which integrate across each of the inner and outer divertor volumes and accounts for the differences in the divertor volumes due to the toroidal geometry. As in Fig.4(b), the out/in D_α ratio is plotted as a function of the sign of B_φ multiplied by an approximate upstream power per particle derived separately for each time window.

With increasing $P_{SOL}/n_{e,\,vol}$ (and hence likely an increasing influence of drifts), there is a strong decrease in the ratio for forward B_φ and rather symmetric recycling in reversed field, independent of the $P_{SOL}/n_{e,\,vol}$. This data therefore supports a drift motion that brings more plasma particles to the inner divertor in forward field (increasing the density there) and to the outer divertor in reversed B_φ. Such conclusions are also consistent with those based on Helium enrichment experiments [28]. One candidate satisfying this criteria is the radial $E_\theta \times B$ drift in the SOL, perhaps in association with the poloidal $E_r \times B$ drift in the PFR which, for reversed B_φ, would drive particles from inner to outer divertor. These radial SOL drifts are expected to be dominant in high recycling plasmas [29] - the case for many of the database discharges. Figure 5(b) is an attempt to summarise the effect of field reversal on impurity production in the divertor using the out/in ratio of CIII visible light emission (at 465nm) normalised in each case to the local D_α emission and therefore a crude measure

of the carbon production rate. In reversed B' the ratio is again rather symmetric, but favours the outer target in forward field.

The interpretation of this data is not straightforward, since the CIII (and D_α) emission is integrated over the entire divertor volume and depends in a complex way on the carbon transport and production mechanisms, the latter being by physical or chemical sputtering, each of which operates more-or-less efficiently depending on plasma conditions. It is interesting to note, however, that EDGE2D modelling using a transport pinch to simulate the forward field case [19] reproduces the trends with PSOL of both the D_α and CIII ratios seen in Fig.5(b) and the energy asymmetry in Fig.4(a).

Related to the impurity production and/or the source rate is the unexpected observation, illustrated in Fig.6, that reversed field operation leads to the accumulation of a surface layer at the outer target which later disappears gradually following the return to forward field plasmas [24]. This phenomenon, diagnosed using IR thermography as an anomalously high rate of surface temperature rise in response to an abrupt increase in additional heating power, is always seen at the inner target in JET (also in reversed B_φ), which is well known to be a region of net deposition for forward B_φ operation [30]. In contrast, the outer target in forward field is, by and large, a region of net erosion and the "IR anomaly" is not observed there. It is these surface layers that provide the greatest obstacle to the derivation of heat fluxes from IR temperature measurements, especially on a fast timescale during ELM events [24]. Since the outer divertor plasma is known to be little affected by field reversal, the development of an impurity layer at the outer target during the reversed B_φ campaign would appear to be due at least partly to a net source of impurities flowing into the outer divertor.

That this may be a plausible scenario can be shown qualitatively by a returning to simulation results drawn from the same code runs that have been discussed in Section 3.2. Fig.7 compiles the code prediction for the *poloidal* distribution of parallel SOL flow, again expressed in terms of $M_{||}$ for a number of separatrix distances and for both directions of B_φ in matched, low density conditions.

The simulated forward field flow is directed from outer to inner divertor almost across the entire poloidal cross-section. Flow reversal towards the outer target occurs only underneath the outside midplane (when the divertor influence begins to be felt) and even here it remains directed towards the inner divertor close to the separatrix. Section 3.2 has demonstrated that the model flow is by a large factor insufficient to account for the Mach probe measurements and no claim is made here that the flow pattern is quantitatively able to account for the net convection of main chamber released impurities to the inner target. These results do, however, support recent C^{13} injection experiments on JET which find that for forward B_φ, 90% of marker impurities introduced at the vessel top are finally deposited at the inner divertor targets [31].

In reversed B_φ, the poloidal flow pattern is markedly different, exhibiting a strong flow reversal point near the top of the machine, coincidentally very close to the reciprocating probe position. In this case, therefore, the flow is essentially directed equally towards each divertor target from the machine top. Depending on the (complex) details of how impurities released from the main chamber

walls are entrained in the background flow and with the caveat that there are still large discrepancies between the observed and predicted flow strengths, these results are not inconsistent with an enhanced supply of impurities towards the outer divertor in reversed field originating from a (field independent) source at the LFS main chamber wall.

CONCLUSIONS

Results from the most recent reversed field campaign at JET in combination with numerical modelling are providing some valuable insights into the pattern of SOL flows and divertor energy and particle asymmetries. Earlier measurements of strong parallel flow at the top of the machine from outer to inner divertor in normal field operation have been confirmed and improved upon. New data in reversed field show an almost stagnant flow throughout most of the SOL except near the separatrix. The forward field flow is almost an order of magnitude larger than be accounted for by EDGE2D code simulations including all classical drifts. Likewise, the model does not reproduce the flow offset ($M_{||} \sim 0.2$) from outer to inner target seen experimentally for both field directions. A number of avenues are being pursued to increase the predicted EDGE2D forward field flow - the inclusion of anomalous convective pinch terms, ballooning like diffusive particle transport and the perturbing effect of the probe.

Divertor energy asymmetries are observed to be strongly dependent on the sign of B' but not its magnitude. This finding is a direct consequence of radial energy transport which is independent of field direction and which scales inversely with B_{φ}. It is strong evidence for drift effects being the main driver for the observed change in in/out asymmetry with field reversal.

Divertor tile temperature measurements using IR thermography have revealed the build-up of a thermally resistent surface layer on the outer target during reversed field operation, implying that the outer divertor switches from a region of net erosion (the case in forward field) to net redeposition. This new observation is not inconsistent with the rearrangement of the poloidal distribution of parallel SOL flow seen when the field is reversed in EDGE2D simulations including cross-field drifts.

ACKNOWLEDGEMENTS

This work was performed under the European Fusion Development Agreement and was supported in part by the Swiss National Science Foundation, EURATOM and the UK Engineering and Physical Sciences Research Council.

REFERENCES

[1]. Nuclear Fusion **39** (1999) 2137

[2]. G. F. Matthews, these proceedings (PSI-16)

[3]. B. LaBombard et al., these proceedings (PSI-16)

[4]. N. Asakura et al., Nucl. Fusion **44** (2004) 503

[5]. D. N. Hill et al., J. Nucl. Mater **176-177** (1990) 158

[6]. I. H. Hutchinson et al., Plasma Phys. Contr. Fusion **38** (1996) A301

[7]. N. Asakura et al., J. Nucl. Mater **220-222** (1995) 395

[8]. A. V. Chankin et al., Plasma Phys. Contr. Fusion **38** (1996) 1579

[9]. A. Kallenbach et al., Plasma Phys. Contr. Fusion **46** (2004) 431

[10]. S. K. Erents et al, Plasma Phys. Contr. Fusion **42** (2000) 905

[11]. R. A. Pitts et al., Rev. Sci. Instr. 74 (2004) 4644

[12]. C. Silva et al., to be published in Rev. Sci. Instr.

[13]. I. H. Hutchinson, Phys. Fluids **B3** (1991) 847

[14]. S. K. Erents, R. A. Pitts et al, submitted to Plasma Phys. Contr. Fusion

[15]. F. Valsaque et al, Phys. Plasmas **9** (2002) 1806

[16]. R. A. Pitts et al, Proc. 30th EPS Conference on Contr. Fusion and Plasma Phys., St. Petersburg, 7-11 July 2003, ECA Vol. **27A** (2003) P-2.84 R. A. Pitts et al., PSI-16, paper #276 17 of 25

[17]. R. Simonini et al, Contrib. Plasma Phys. **34** (1994) 368

[18]. D. P. Coster et al., these proceedings (PSI-16)

[19]. G. Kirnev et al., these proceedings (PSI-16)

[20]. J. D. Strachan et al., these proceedings (PSI-16)

[21]. W. Fundamenski et al., these proceedings (PSI-16)

[22]. A. Huber et al., these proceedings (PSI-16)

[23]. A. V. Chankin, J. Nucl. Mater **241-243** (1997) 199

[24]. P. Andrew et al., these proceedings (PSI-16)

[25]. W. Fundamenski, S. Sipilä et al, Nucl. Fusion **44** (2004) 20

[26]. S. K. Erents et al., Nucl. Fusion **40** (2000) 309

[27]. J. A. Boedo et al., Phys. Plasmas **7** (2000) 1075

[28]. M. Lehnen et al., to be presented at 31st European Physical Society Conference on Plasma Physics, London, June 28-July 02 2004.

[29]. P. C. Stangeby, A. V. Chankin, Nucl. Fusion **36** (1996) 839

[30]. J. P. Coad et al., J. Nucl. Mater **313-316** (2003) 419

[31]. J. Likonen et al., Fus. Engineering and Design **66-68** (2003) 219

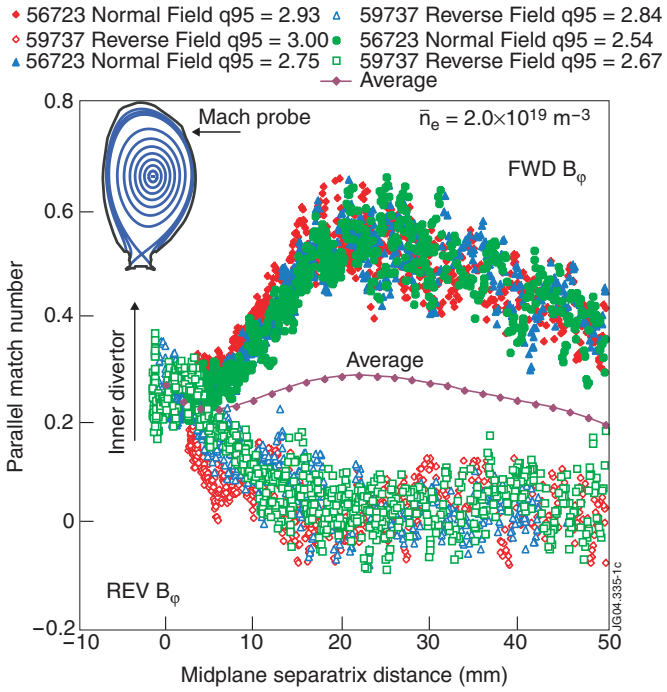

Figure 1: Radial dependence of M|| measured by the RFA probe at the top, LFS of the machine (see inset) in matched, ohmic, low density forward and reversed B' discharges. Data are from three reciprocations into the steady state phase of pulses with a slow B_j ramp.

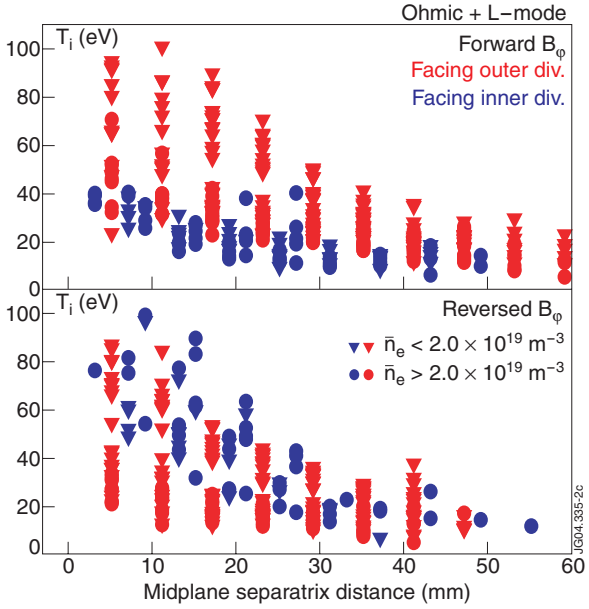

Figure 2: Radial Ti profiles, ordered by density, on each side of the bi-directional RFA probe for a large selection of forward and reversed B_j discharges. The data are obtained mostly from the ohmic phase of each pulse.

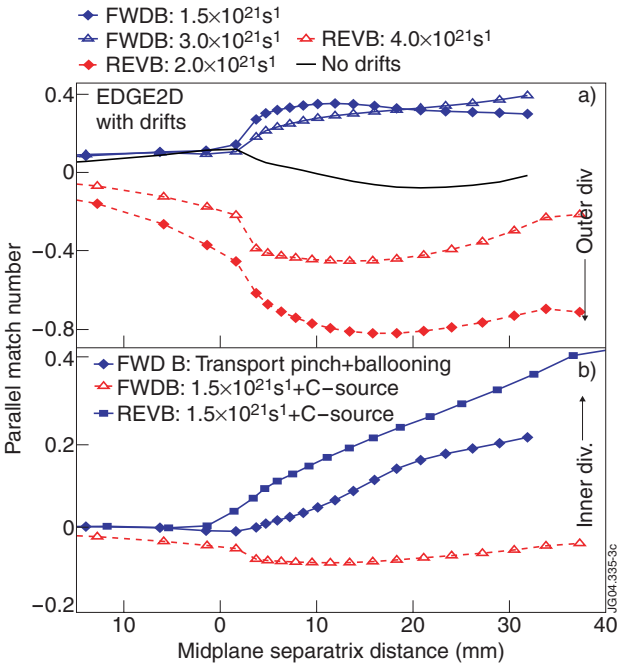

Figure 3: Simulation results for M||(r) at the RFA probe location (mapped to the midplane) from the EDGE2D/Nimbus code package: (a) with/without drifts and for two values of upstream density with drifts, (b) including two proposed mechanisms for increasing the predicted forward field flow.

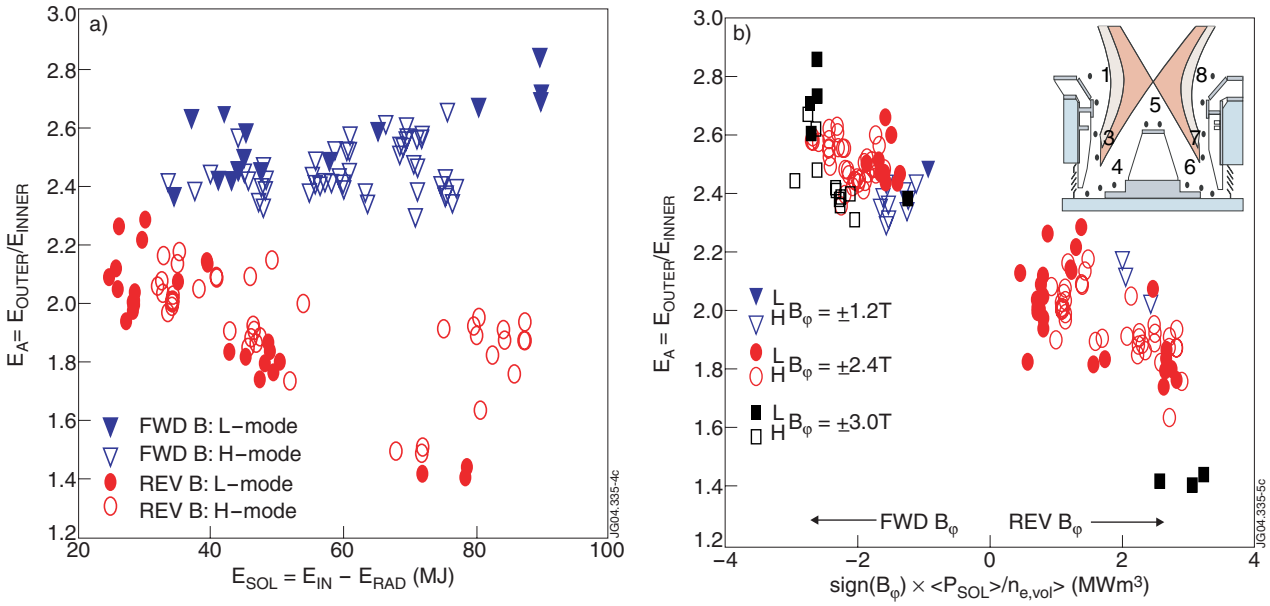

Figure 4: Divertor tile thermocouple (see inset in (b)) data from the DOC-L database of forward and reversed B_j pulses: (a) dependence of the out/in energy asymmetry (EA) on energy to the divertor (computed using energies to the vertical tiles 1+3 7+8), (b) scaling of EA with upstream power/per particle.

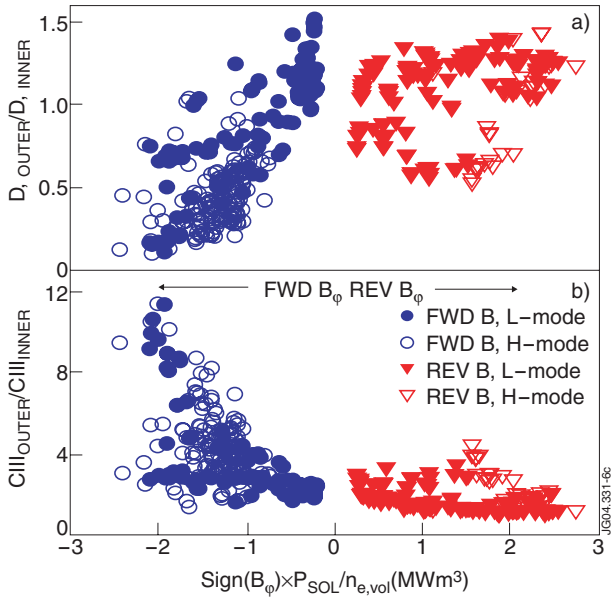

Figure 5: Evidence for symmetrisation of divertor recycling and carbon emission in reversed field: (a) ratio of integrated outer and inner D_a emission, (b) ratio of approximate carbon production rates.

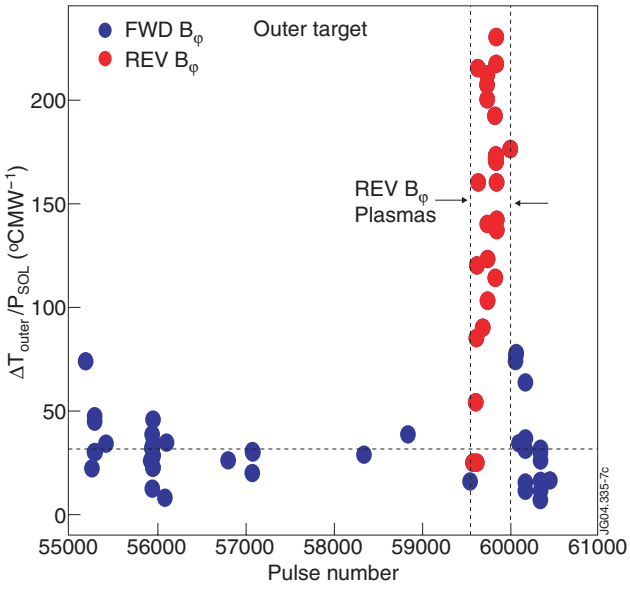

Figure 6: Illustrating the appearance of an anomaly at the outer target during reversed B_j in the measured IR surface temperature response to steps in power input to the SOL [24].

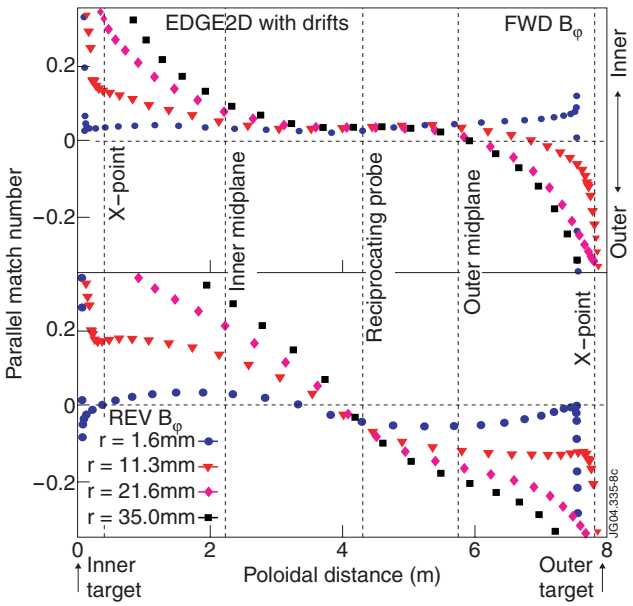

Figure 7: EDGE2D simulation results including drifts for the poloidal distribution of $M_{||}$ at four radial positions in the SOL for forward and reversed B_j. The radial profiles in Figure 3(a) originate from the same code runs.